Nonequilibrium dynamics and action at a distance in transcriptionally driven DNA supercoiling

Yair A. G. Fosado[a,1], Davide Michieletto[b,c], Chris A. Brackley[b], and Davide Marenduzzo[b,1]

[a]Department of Physics and Mathematics, Aoyama Gakuin University, Kanagawa 252-5258, Japan; [b]Scottish Universities Physics Alliance, School of Physics and Astronomy, University of Edinburgh, Edinburgh, EH9 3FD, United Kingdom; and [c]Medical Research Council Human Genetics Unit, Institute of Genetics and Molecular Medicine, University of Edinburgh, Edinburgh EH4 2XU, United Kingdom

Edited by Herbert Levine, Northeastern University, Boston, MA, and approved December 30, 2020 (received for review March 27, 2019)

We study the effect of transcription on the kinetics of DNA supercoiling in three dimensions by means of Brownian dynamics simulations of a single-nucleotide–resolution coarse-grained model for double-stranded DNA. By explicitly accounting for the action of a transcribing RNA polymerase (RNAP), we characterize the geometry and nonequilibrium dynamics of the ensuing twin supercoiling domains. Contrary to the typical textbook picture, we find that the generation of twist by RNAP results in the formation of plectonemes (writhed DNA) some distance away. We further demonstrate that this translates into an "action at a distance" on DNA-binding proteins; for instance, positive supercoils downstream of an elongating RNAP destabilize nucleosomes long before the transcriptional machinery reaches the histone octamer. We also analyze the relaxation dynamics of supercoiled double-stranded DNA, and characterize the widely different timescales of twist diffusion, which is a simple and fast process, and writhe relaxation, which is much slower and entails multiple steps.

DNA topology | supercoiling | transcription | nonequilibrium physics

The double-stranded nature of DNA endows it with the properties of an elastic rod with both bending and twisting rigidities (1, 2). Mechanical manipulation which overwinds or underwinds the double helix leads to torsional strain that can be relieved by the DNA writhing onto itself (2). This phenomenon is a consequence of a topological conservation law: If the DNA is in a closed loop, or its ends are fixed, the number of times the two strands wind around each other—the linking number (Lk)—is a topological invariant. The White–Fuller–Calugarenau (WFC) theorem (3–5) states that the linking number of a DNA helix can be written as the sum of two contributions, its "twist" (Tw) and "writhe" (Wr), $\mathrm{Lk} = \mathrm{Tw} + \mathrm{Wr}$. The twist can be thought of as the number of times the vector joining DNA nucleotides rotates around the backbone, whereas the writhe essentially counts the (signed) self-crossing of the backbone (2). In its relaxed state, a DNA double helix will have a unit linking number for every ~ 10.5 base pairs (bps); a molecule with a linking number different from this is said to be supercoiled.

Bacterial plasmids are kept in a negatively supercoiled state with important consequences for gene expression (6). In eukaryotes, the modulation of DNA twist along the chromosome is also thought to play a role in regulating gene expression (7). Irrespective of the organism, in vivo DNA is constantly being remodeled by proteins, such as RNA polymerase (RNAP), that drive the system away from equilibrium by applying forces and torques of the order of 25 pN (8, 9) and 11 pN nm (10), respectively. The role of RNAP in creating supercoiling is broadly associated with the "twin supercoiling domain" (TSD) model (11, 12). This predicts the formation of positive supercoils ahead of RNAP and negative supercoils in its wake; further, such dynamically generated supercoiling has been conjectured to play a regulatory role in gene expression either through the twist dependence of polymerase–DNA interactions (13, 14), or via supercoiling-mediated generation of DNA loops (6). Although the TSD model was proposed over 30 years ago, its consequences in vivo are far from understood.

In this work, we use three-dimensional (3D) Brownian dynamics (BD) simulations of a single-nucleotide–resolution model for DNA (15, 16) to study the generation of TSDs by means of RNAP transcription. Our simulations go beyond the 1D description of RNAP-driven supercoiling used in recent models (13, 14, 17) as well as earlier studies using a twistable wormlike chain model for DNA and an effective external torque to model the effect of the RNAP (18, 19). Contrary to typical textbook diagrams which show twist or writhe being generated close to RNAP on both sides, we discovered that writhe nucleates into plectonemes that appear at a considerable distance from the polymerase; this allows for an "action-at-a-distance" phenomenon, where transcription at one point can affect the binding of proteins—such as histones or other RNAPs—elsewhere. Additionally, we study twist and writhe relaxation in the absence of RNAP and find they differ vastly, both quantitatively and qualitatively: Twist diffuses away rapidly, whereas writhe relaxation is much slower and entails at least two distinct timescales. Our results challenge the TSD paradigm and motivate further efforts to dissect the dynamics of supercoiling in single-molecule experiments.

Results

The Model. We simulate a DNA loop by using a recently developed single-nucleotide–resolution model for double-stranded

Significance

Positive and negative supercoiling refers to the overwinding or underwinding, respectively, of a DNA double helix. Supercoiling is important and ubiquitous, as all cells, from bacterial to human, deploy proteins to keep their genome negatively supercoiled to facilitate transcription and replication. Additionally, as a polymerase transcribes a gene, its action generates twin domains of supercoils of opposite sign. Here we characterize, by simulations, the three-dimensional geometry of such domains, and show that supercoiling can be exploited to act at a distance on DNA-binding proteins, for instance, unwrapping a nucleosome long before the polymerase reaches it. We also quantify the dynamics of double-stranded DNA supercoiling, and the striking timescale separation between the diffusive relaxation of twist and writhe.

Author contributions: Y.A.G.F., D. Michieletto, C.A.B., and D. Marenduzzo designed research; Y.A.G.F., D. Michieletto, and C.A.B. performed research; Y.A.G.F., D. Michieletto, C.A.B., and D. Marenduzzo analyzed data; and Y.A.G.F., D. Michieletto, C.A.B., and D. Marenduzzo wrote the paper.

The authors declare no competing interest.

This article is a PNAS Direct Submission.

[1]To whom correspondence may be addressed. Email: gtzyair@gmail.com or dmarendu@ph.ed.ac.uk.

This article contains supporting information online at https://www.pnas.org/lookup/suppl/doi:10.1073/pnas.1905215118/-/DCSupplemental.

Published March 1, 2021.

DNA (dsDNA) that fully accounts for its double helical structure, denaturation, and elastic properties (15, 16). While neglecting hydrodynamic interactions, the model also qualitatively captures the dynamics of supercoiled dsDNA (16) (see *SI Appendix* for more details). Unless otherwise stated, we consider an $L = 1{,}000$-bp-long loop in which the linking number is equal to the "relaxed" value $\mathrm{Lk} = \mathrm{Lk}_0 = L/p$, with p as the pitch of the DNA helix (10 bp in our model).

An RNAP is modeled as a rigid body consisting of a ring which encircles the double helix and a "crossbar" which passes between the two DNA strands and is anchored to the ring on each side (Fig. 1*A*). The dsDNA segment passing through the RNAP experiences an active force, F_p, directed perpendicular to the plane of the ring, which drives the relative motion of RNAP and DNA at a velocity v. The steric interaction between the crossbar and the DNA beads forces the opening up of the double strand and leads to positive twisting (overwinding) in front of the RNAP and negative twisting (underwinding) behind. Our model correctly captures the mechanical action of an elongating RNAP which must unwind a section of the helix in order to "read" the nucleotides (1, 20). We quote velocities in units of $\mathrm{bp}/\tau_{\mathrm{Br}}$, where τ_{Br} is the Brownian time—which is proportional to the time needed for a DNA bead to diffuse its own size. The latter can vary between ~ 2.3 ns in a water-like in vitro environment and ~ 1 μs in vivo where crowding and DNA-associating proteins slow down motion dramatically (*SI Appendix*), although the fact that our model disregards solvent-mediated hydrodynamic interactions hinders a fully quantitative mapping to real units. Full details of the simulation units, and the DNA and RNAP models, are given in *SI Appendix*. Note that the linking number added or removed by the RNAP per unit time is given by v/p.

For simplicity, we focus on a geometry where the RNAP is fixed in 3D space; this could either mimic an in vitro setup or capture the fact that in vivo RNAPs are associated with a large elongation complex which experiences a larger rotational drag than the DNA (21). Qualitatively similar results are obtained for a moving RNAP, provided that the rotational drag (whose value is not well characterized in vivo) is sufficiently large (*SI Appendix*, section 3 and Fig. S3).

RNAP Elongation Creates Asymmetric TSDs. Within the crowded environment of the cell, binding of large protein complexes or the formation of loops can restrict DNA rotation at specific sites, impeding the transmission of twist (20). To mimic this constraint, we introduce a "topological barrier" (TB)—a section of DNA

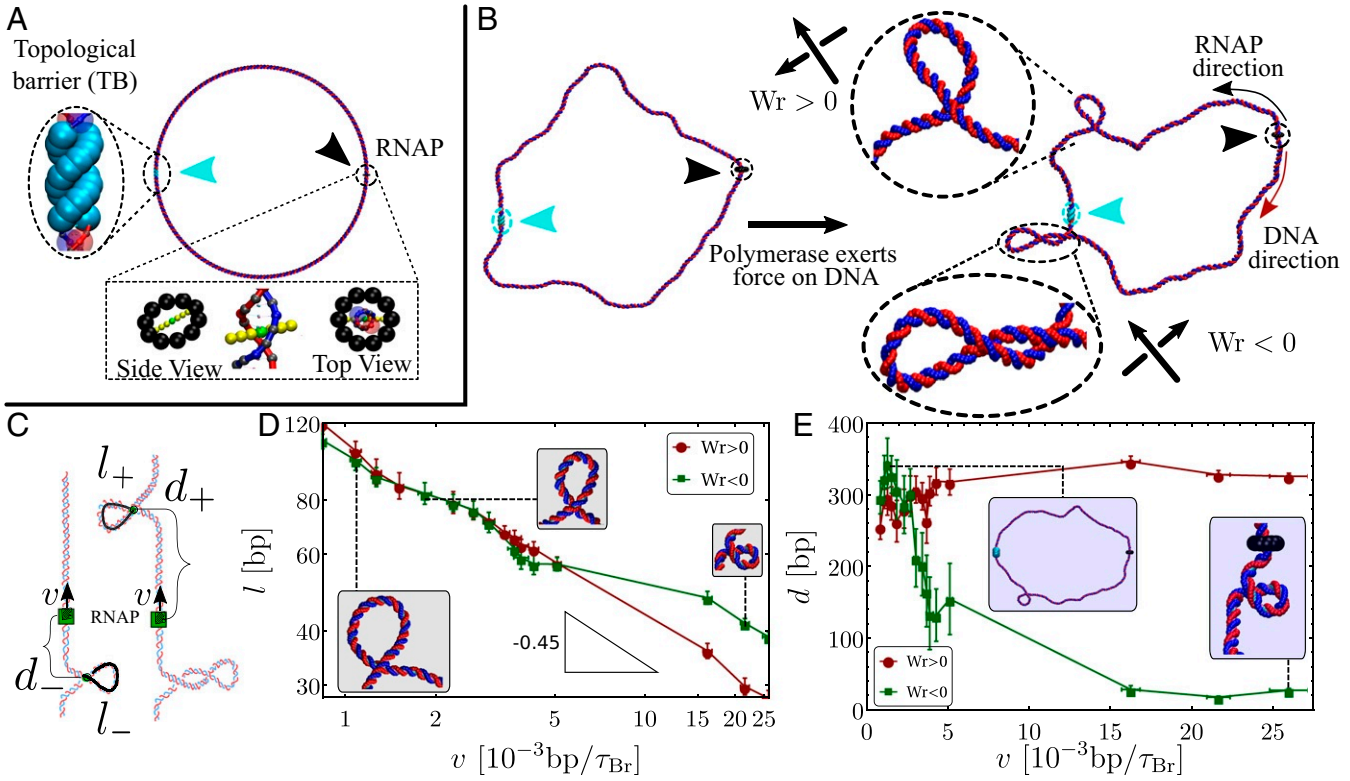

Fig. 1. Simulating twin supercoiled domains. (*A*) An $L = 1{,}000$-bp dsDNA molecule is initialized as a circle with $\mathrm{Lk} = \mathrm{Lk}_0$. An RNAP is modeled as a rod orthogonal to the DNA backbone and a ring which encircles it (*SI Appendix, Supporting Information Text* and Figs. S1 and S2). The position of the RNAP is permanently fixed in 3D space (we present simulations for a moving RNAP in *SI Appendix, Supporting Information Text* and Fig. S3), and a TB (a section of DNA which cannot rotate) is positioned at $L/2$ and impedes twist transmission. Results obtained for different lengths of the DNA molecule and positions of the TB are shown in *SI Appendix*. (*B*) After an initial simulation run to allow the DNA to reach an equilibrated conformation (left), the RNAP is activated: All DNA beads which are within a distance of 0.5 nm from the center of the RNAP experience a force of magnitude F_p directed perpendicular to the plane of the ring. This causes the relative movement of the RNAP at a speed v. In turn, supercoiled domains emerge and plectonemes of opposite writhe form at a considerable distance from RNAP (right). Cyan and black arrowheads indicate the TB and RNAP, respectively. (*C*) Schematic of the geometry of the TSD, defining the distances d_+ and d_- and the respective lengths l_+ and l_-. (*D*) Log–log plot of the length l of the plectoneme at its first appearance as function of v. Red and green points show positive and negative writhe, respectively. Lines are a guide for the eye. We observed that, at low velocities, the length of the plectoneme follows the relation $l \approx v^{-0.45}$ regardless of the sign of Wr. At high velocities, the slope decreases, particularly for $\mathrm{Wr} < 0$, probably indicating the larger bending energy cost of forming smaller plectonemes. Snapshots are shown as *Insets*. (*E*) The contour length d from the RNAP to the first plectoneme crossing at the time of its first appearance is plotted as a function of v. Green points are for $\mathrm{Wr} < 0$, and red points are for $\mathrm{Wr} > 0$; connecting lines are a guide for the eye. Snapshots are shown as *Insets*.

which is not free to rotate and thus effectively acts as a reflecting barrier for twist (Fig. 1*A*). In this context, we investigate the effect of twist generation by examining different values of v for a DNA molecule which was initially topologically relaxed (Fig. 1*B*, left).

Once a sufficiently large amount of supercoiling has been introduced by the RNAP, we observe the emergence of plectonemic structures on each side. Unexpectedly, we discover that plectonemes can appear at large distances from the RNAP complex, and that each can store a different amount of writhe. For instance, to the right in Fig. 1*B*, we show a configuration obtained after the RNAP has traveled 3.4 turns of the helix: Plectonemes with $\mathrm{Wr}=+1$ and $\mathrm{Wr}=-2$ have formed ahead of and behind the RNAP, respectively. This is contrary to the usual TSD picture, which would suggest equal and opposite writhing on each side close to the RNAP (11). Although the writhe within the plectonemes is unbalanced, the total linking number must still be conserved to satisfy the WFC theorem, that is, $\mathrm{Lk}(t)=\mathrm{Lk}_0=\mathrm{Tw}(t)+\mathrm{Wr}(t)$ (2). We verify this is the case by computing the global twist and writhe as a function of time (*SI Appendix*, Fig. S4 and *Supporting Information Text*). This calculation indicates that not all of the writhe is stored in the plectonemes, but part of it is delocalized over the whole polymer (as counting positive and negative crossings in plectonemes would give $\mathrm{Wr}=-1$, whereas, overall, we measure $\mathrm{Wr}\approx\mathrm{Wr}_0=0$).

The Geometry of Transcription-Driven Plectonemes Depends on *v*. To understand the formation of plectonemes more quantitatively, we developed a strategy to monitor both their position and length as they are generated (*SI Appendix*, *Supporting Information Text* and Fig. S5). First, we find that the larger the velocity the smaller the plectoneme (Fig. 1*D*); specifically, its size $l\approx v^{-\alpha}$ with $\alpha\approx 0.45$ for small v, and smaller for large v. Second, we find that, depending on v, there are two regimes for the distance d between the RNAP and the plectoneme (Fig. 1*E*). For large velocities ($v\geq 2.5\times10^{-3}$ bp/τ_{Br}), d depends on the sign of the supercoiling: For $\mathrm{Wr}>0$, that is, in front of the RNAP, d increases with the speed, whereas, for $\mathrm{Wr}<0$, that is, behind the RNAP, it instead decreases with v. We attribute this to the tension experienced by the DNA in front of the RNAP as it is "reeled in": The backbone is straightened, and writhing is suppressed (Fig. 1 *E*, *Right Inset*; see also ref. 22). At the same time, there is an accumulation of DNA under compression behind the RNAP, and this can more readily form a plectoneme.

For small velocities ($v<2.5\times10^{-3}$ bp/τ_{Br}), we observe a markedly different behavior: The RNAP does not exert enough force to immediately break the attraction between the DNA strands (*SI Appendix*, Fig. S6), and the timescale associated with pulling a segment of DNA is comparable to that of its 3D relaxation. The RNAP and the TB give rise to a reduced freedom of the DNA to move and rotate, so plectonemes are less likely to form in their immediate vicinity. In this regime, there are no further constraints on plectoneme formation, meaning that, on average, they appear close to the halfway point between the RNAP and TB, as would be expected by symmetry (Fig. 1*E*). We expect this regime to occur for values of F_{p} and v relevant to RNAP in vivo (*SI Appendix*).

In our simulations, the supercoiling density in the TSDs at which the $\mathrm{Wr}>0$ plectoneme forms is typically larger than that at which the $\mathrm{Wr}<0$ one appears (*SI Appendix*, Fig. S9*A*). The main reason is, again, that the positively supercoiled plectoneme is under tension, which increases the supercoiling density required for writhing. This finding is in agreement with the observation in ref. 23 that negatively supercoiled DNA is more difficult to twist (but easier to bend) compared to positively supercoiled DNA. The force-dependent values of supercoiling densities at which plectonemes form are $|\Delta\mathrm{Lk}/\mathrm{Lk}|\approx 0.01-0.3$, which can be readily achieved for DNA in vitro or in vivo. In most cases, we also find that the negatively supercoiled plectoneme is the first to form (*SI Appendix*, Fig. S9*B*).

We have also studied how the length of the DNA and the position of the TB affect our findings. For a setup with a ring with $L=2{,}000$ bp, and with the TB placed opposite the RNAP at $t=0$, we obtain analogous results to those in Fig. 1 (*SI Appendix*, Fig. S7). When varying the position of the TB (*SI Appendix*, Fig. S8), we detected two differences: The first plectoneme that appears in the simulation is now that for which the RNAP is initially closer to the TB, and the plectoneme size is slightly affected by the TB position. In all cases, however, plectonemes appear far from the RNAP, and the TSDs are markedly asymmetric (*SI Appendix*, Figs. S7 and S8). While we have focused, for concreteness, on the geometry of plectonemes when they first form, we have monitored their overall dynamics as well. The kymographs in *SI Appendix*, Fig. S10 show that plectoneme mobilities and growth rates also greatly vary with v.

Nucleosomes Are Unwrapped by RNAP at a Distance. We reasoned that the above-mentioned "action at a distance" might mechanically affect the binding of a protein on DNA (24). To test this hypothesis, we consider the basic building block of eukaryotic chromatin, the nucleosome, and model a histone octamer as a spherical bead of diameter 10 nm, with 20 "sticky patches" tracing a left-handed helical path on its surface covering exactly 1.7 turns (25). By introducing a short-range attraction between the patches and the DNA beads, modeling screened electrostatic interactions, we can readily simulate the self-assembly of a nucleosome (Fig. 2*A*).

We initialize the system as a loop of DNA with $\mathrm{Lk}=\mathrm{Lk}_0$, containing an inactive RNAP ($F_p=0$) and an octamer, positioned at the opposite side of the loop. We observed that, as the DNA wraps around the octamer, the topology of the nucleosome is in agreement with the "linking number paradox" (2, 26): While the DNA completes 1.7 turns around the histone core, the wrapped section is slightly overtwisted (Fig. 2*A*), resulting in a net linking number storage of about -1 per nucleosome (2). Once the nucleosome has formed and the DNA is equilibrated (Fig. 2*A*), we introduce a TB and activate the RNAP. The TB isolates the nucleosome from supercoils coming from one direction, and we can dissect the role of negative and positive supercoiling by considering an RNAP moving toward or away from the nucleosome.

In Fig. 2 *B*, *Right*, we plot the averaged local twist $\langle\theta(x)-\theta_0\rangle$ at a fixed time after RNAP activation at key locations along the DNA (at the nucleosome, at the TB, and within the supercoiled domains). Remarkably, when the nucleosome is subject to RNAP-driven positive supercoiling, it becomes destabilized, and the DNA unwraps long before the RNAP reaches it (Fig. 2 *B*, *Left*). Conversely, when the nucleosome is subject to negative supercoiling, there is no unraveling, and, instead, the nucleosome structure becomes more stable (Fig. 2*C* and *SI Appendix*, Fig. S11). The average timescale (after activation of the RNAP) at which the detachment occurs is $t=0.7\times10^4\tau_{\mathrm{Br}}$. The average distance traveled by the polymerase during this time is 14.26 bp, and therefore $\Delta\mathrm{Lk}\approx 1.43$. Given the TSD geometry at the time of unraveling, the corresponding supercoiling density is $\Delta\mathrm{Lk}/\mathrm{Lk}_0=0.034$, easily achievable for RNAP in vivo.

Our simulations not only agree with previous observations of transcription-driven nucleosome eviction in vitro (27) but also suggest that the removal of obstacles in front of an advancing RNAP may take place without any direct contact with it through an "action-at-a-distance" mechanism which exploits the traveling of supercoiling along the DNA.

Two Modes of Supercoiling Relaxation: Diffusing Twist. Having observed that RNAP-driven supercoiling spreads along the DNA, we now use our 3D simulations to dissect the mechanisms

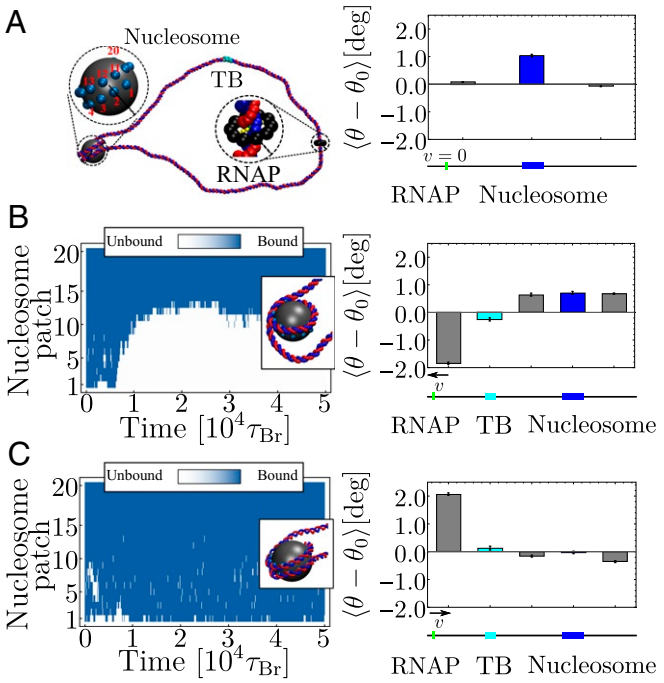

Fig. 2. RNAP-generated supercoiling disrupts nucleosomes from a distance. (*A*) Initial configuration for an equilibrated 1,000-bp dsDNA ring where a fully wrapped nucleosome is positioned opposite the RNAP. *Left Inset* shows the model nucleosome, with patches following a left-handed path with 1.7 dsDNA turns. *Right Inset* shows how the twist angle $\theta(n)$ varies around the loop with respect to $\theta_0 = 36°$ in three different regions (depicted schematically at the bottom of the plot): between the RNAP and the left of the nucleosome, at the nucleosome, and to the right of the nucleosome. The region of the DNA attached to the nucleosome is the most overtwisted, in agreement with the linking number paradox (2). (*B* and *C*) A TB is positioned at bp 230 to 240 to isolate the nucleosome from supercoiling traveling from one side, and the RNAP is activated. *Left* shows the attachment of the DNA to the histone patches via a kymograph (blue indicates a patch is bound; white indicates it is unbound). *Right* shows the local twist $\langle\theta(n)-\theta_0\rangle$ at a time $t = 10^4\ \tau_{Br}$ after the RNAP is activated (averaged over 50 independent simulations). This is computed at five different regions, again shown schematically underneath the plots. The TB twist displays a small, nonzero deviation from θ_0, because we restrict its rotation only after equilibration. In *B*, the RNAP is oriented such that positive supercoils travel toward the nucleosome (the TB isolates it from negative supercoils): The DNA progressively unwraps from the nucleosome. After $t = 10^4\ \tau_{Br}$, the region behind the RNAP is undertwisted, whereas the region in front is overtwisted by $\sim 0.5°$ per bp. In *C*, the direction of the RNAP is reversed such that negative supercoils now reach the nucleosome: The DNA remains stably wrapped throughout the simulation.

of twist and writhe relaxation. First, we consider twist relaxation. We initialize a 1,000-bp dsDNA loop in a nonrelaxed state with $\mathrm{Tw} - \mathrm{Tw}_0 = 1$. This is done by fixing the twist angle contained within a short (40 bp) segment at $\theta(n) = 45°$, away from the preferred value of $\theta_0 = 36°$; we then run a simulation preserving this constraint to generate an equilibrated conformation with a locally overtwisted segment. By releasing the constraint, we study the relaxation of twist by monitoring its local value along the DNA (Fig. 3*A*).

We find that twist relaxation can be fitted by an analytical solution of the diffusion equation, $\partial_t\theta(x,t) = D_{\mathrm{Tw}}\nabla^2\theta(x,t)$, with initial condition $\theta(x,0) = 45°$ if $x_i < x < x_f$, and $\theta(x,0) = \theta_0 = 36°$ otherwise (*SI Appendix*). By fitting $\theta(x,t)$ to our simulation data, we extract the diffusion coefficient $D^+_{\mathrm{Tw}} = 540 \pm 36$ $\mathrm{bp}^2/\tau_{\mathrm{Br}}$. A comparable value of $D^-_{\mathrm{Tw}} = 493 \pm 32$ $\mathrm{bp}^2/\tau_{\mathrm{Br}}$, was obtained for an undertwisted DNA, initialized with $\theta_n = 27°$ within the same segment (between points x_i and x_f). These numerical estimates are robust for different lengths of the overtwisted/undertwisted segment. While the values of D^+_{Tw} and D^-_{Tw} are compatible within the errors, there is no reason why the

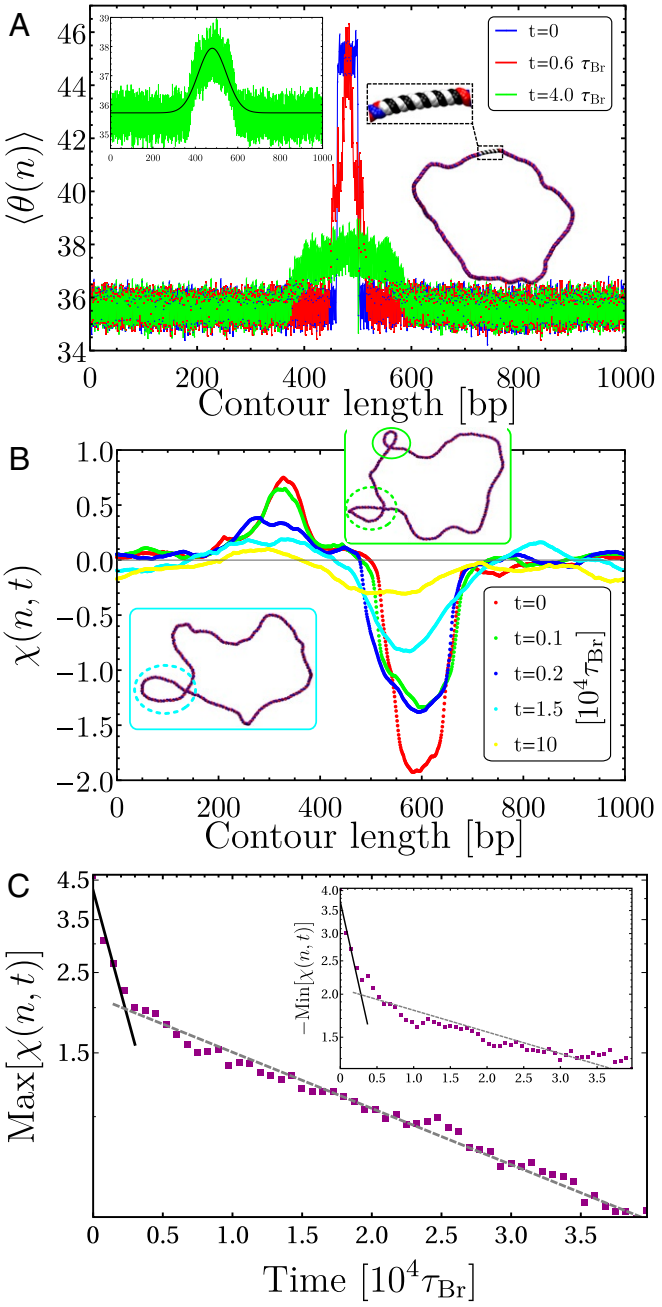

Fig. 3. Twist and writhe relaxation in the absence of RNAP. (*A*) Local twist angle $\theta(n)$ averaged over 1,000 short simulations. Different colors indicate different times after the constraint was removed. In *Left Inset*, the data at $4\tau_{Br}$ are shown in green, and the black line is a fit to the solution of the diffusion equation. A snapshot of the initial configuration is shown in *Right Inset*. (*B*) Local writhe $\chi(n,t)$ (*SI Appendix*) at different times after removing the TB and the RNAP from a supercoiled DNA loop. *Insets* show snapshots of configurations at $t = 0.1 \times 10^4\tau_{Br}$ and $t = 1.5 \times 10^4\tau_{Br}$. (*C*) Log-linear plot of the maximum of $\chi(n,t)$ as a function of time. Purple squares are from simulations, and lines represent fits with exponentially decaying functions $e^{-t/\tau}$, with $\tau = \tau_1^+$ and τ_2^+ for the two regimes. *Inset* shows a similar plot for the minimum of $\chi(n,t)$. More details are provided in *SI Appendix*, and *SI Appendix*, Figs. S12 and S14 show similar plots for different initial configurations.

two should be equal, as a finite overtwist and undertwist are not related by a simple symmetry (16, 28).

Two Modes of Supercoiling Relaxation: Glassy Writhe. To study the relaxation of writhe, we consider initial configurations which display stable plectonemic structures (localized writhe) and a twist which is close to the relaxed value ($\theta(n) \approx \theta_0$). To achieve this, we use configurations generated in our TSD simulations (such as shown to the right in Fig. 1*B*); we remove both the RNAP and TB and then monitor the local writhe $\chi(n,t)$ (29, 30) (*SI Appendix*) as the molecule relaxes. Typical profiles for $\chi(n,t)$ at different times $t>0$ are shown in Fig. 3*B*; the peaks and troughs identify positively and negatively writhed plectoneme tips, respectively, and we quantify their evolution by recording the maximum and minimum values of $\chi(n,t)$ (29).

We discover that the relaxation of plectonemes occurs in two steps: an initial fast relaxation followed by a slower decay at longer times (Fig. 3*C*). This behavior is due to high levels of writhe stored in the plectonemes; the latter carry conformational stress that is quickly released as soon as the DNA is allowed to relax. At later times, the remaining writhe becomes delocalized (as indicated by the broadening of the peaks in $\chi(n)$), which entails a lower conformational stress leading to a slower decay. (A more quantitative analysis supporting this interpretation is provided in *SI Appendix*, Fig. S16.) We find that the fast and slow relaxations are well fitted by two exponential decays (Fig. 3*C*), where the second relaxation timescale is about an order of magnitude larger than the first.

Our results point to an intrinsic asymmetry between positive and negative writhe, with negatively supercoiled plectonemes relaxing more slowly. Thus, we find that the average timescales of positive writhe relaxation are $\tau_1^+ \approx 2.9\times10^3\tau_{\rm Br}$ and $\tau_2^+ \approx 29\times10^3\tau_{\rm Br}$, whereas, for negative writhe, we measure $\tau_1^- \approx 4.4\times10^3\tau_{\rm Br}$ and $\tau_2^- \approx 44.5\times10^3\tau_{\rm Br}$ (see *SI Appendix*, *Supporting Information Text* and Table S1 for details and additional results). Since there is no energy difference between a positively and negatively writhed configuration, this asymmetry points to a writhe relaxation pathway which involves an intermediate conversion to a twist deformation which is sufficiently strong that the harmonic approximation—according to which the behavior of overtwist/undertwist is symmetric—breaks down (16, 28).

Our observations suggest that supercoiling relaxation occurs through two distinct mechanisms: twist diffusion and writhe dissipation. While the former takes place on very short timescales (associated with a large $D_{\rm Tw}\simeq 500\ {\rm bp}^2/\tau_{\rm Br}$), for the latter we estimate $D_{\rm Wr}\approx l^2/(\tau_1+\tau_2)\sim {\rm bp}^2/\tau_{\rm Br}$ (with $l\approx 100$ bp as the initial plectoneme size), over two orders of magnitude smaller than $D_{\rm Tw}$. This difference arises because writhe relaxation requires global conformational changes which are not necessary to dissipate twist. The existence of a large difference between twist and writhe dynamics is in line with previous predictions obtained with scaling theory and simulations with twistable worm-like chains (18, 19, 31).

Transcription without Topological Constraints. While it is reasonable to assume that in vivo DNA is subject to topological constraints similar to those imposed by our TB, such constraints may be absent for in vitro setups. We therefore ask whether, in the absence of a TB, RNAP-driven supercoiling would simply travel around the DNA loop as twist and annihilate without converting to writhe. To test this, we measure, as a function of time, the total unsigned writhe $\zeta(t)$ (*SI Appendix*) generated by an RNAP in a DNA loop with no TB. This order parameter quantifies the appearance of DNA crossings, irrespectively of their sign (29, 30), and is thus nonzero only in the regime in which plectonemes form.

Our simulations show that $\zeta(t)$ reaches a steady-state $\bar{\zeta}$ at large times and, when plotted as a function of the velocity, $\bar{\zeta}$ shows a transition between a relaxed ($\bar{\zeta}\approx 0$) and a writhed ($\bar{\zeta}>0$) regime at different velocities. The value of the velocity at the transition (v^*) depends on the size of the ring (Fig. 4). As expected, for larger loops, the twist has to diffuse over a greater distance, so $v^*(L)$ decreases with the DNA length L.

In line with ref. 13, we can estimate the extent of residual positive or negative supercoiling induced by an elongating RNAP as $vL/D_{\rm Tw}$, where we use the twist diffusion coefficient, as, initially, there is no writhe. Based on ref. 22, and in line with the results in *SI Appendix*, Fig. S9*A*, plectonemes should start forming when the supercoiling density exceeds ~ 0.01. This criterion suggests plectoneme formation should start from $v\approx 0.01, 0.005$, and $0.0025\ {\rm bp}/\tau_{Br}$ for $L=500, 1{,}000$, and 2,000 bp, respectively, in fair agreement with our simulations. This simple argument disregards the conformational dynamics of the polymer and, in particular, the diffusion of tension along the molecule. Estimating the latter as $\sim\sigma^2/\tau_{Br}\approx 10\ {\rm bp}^2/\tau_{\rm Br}$, we reason that this contribution may affect our estimate for residual supercoiling, and introduces the asymmetry between plectonemes in front of and behind the RNAP as in the case with the TB.

Although we expect that, in vivo, the velocity of an elongating RNAP should be relatively constant, these results demonstrate that its ability to generate plectonemes or affect protein binding depends on the relative rate of supercoil injection and dissipation (the latter being determined by the length of DNA and any topological constraints it is subject to).

Discussion

In this work, we used a single-nucleotide–resolution coarse-grained model for dsDNA to study the nonequilibrium generation and dynamics of supercoiling by RNA polymerase. Importantly, as our simulations resolve the 3D supercoiling dynamics of a dsDNA molecule and the action of the RNAP, they complement and go beyond previous works studying related phenomena with a twistable worm-like chain model subject to an effective torque (18, 19). Our simulations confirm that, when the rotational motion of the polymerase is hindered, its transcriptional activity generates TSDs whereby DNA in front of the RNAP becomes positively supercoiled, and the DNA behind it becomes negatively supercoiled (11).

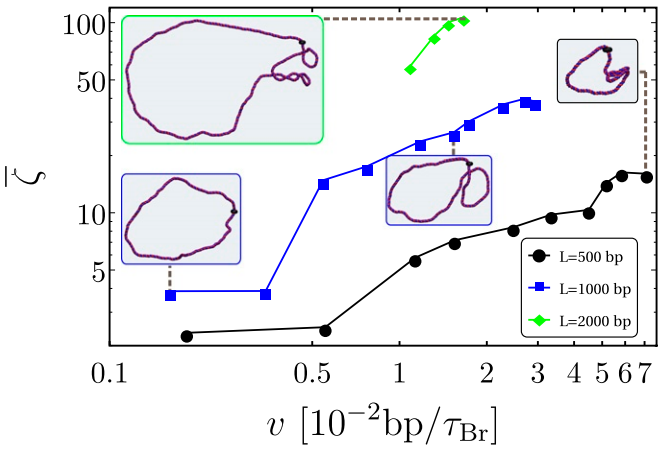

Fig. 4. Log–log plot showing the steady-state unsigned writhe $\bar{\zeta}$ as function of the RNAP velocity from simulations without a TB. Values for DNA molecules of lengths $L=500$, 1,000, and 2,000 are shown. Lines connecting points are a guide for the eye. *Insets* show typical configurations for $F_p=5$ ($v=0.07$) with $L=500$ bp, $F_p=0.5, 3$ ($v=0.0016, 0.015$) with $L=1{,}000$ bp, and $F_p=5$ ($v=0.017$) with $L=2{,}000$ bp. Forces are quoted in units of ϵ/σ, and velocities are in units of bp/τ_{Br}. The same force produces lower velocities for longer chains.

The first main result of our work is that RNAP elongation can trigger an "action at a distance." Contrary to typical textbook pictures (11), we found that the generated twist quickly diffuses away from the RNAP and generates writhe (in the form of plectonemes) some distance away. When the associated length scale, D_{Tw}/v (with v as the speed of the RNAP), is much larger that the size of the DNA molecule, the position of the plectonemes is mainly determined by the distance to the closest topological barrier; when this length scale is small (or, equivalently, the RNAP speed is large), there is symmetry breaking, and plectonemes in front of the RNAP (where DNA is under tension) form farther away, whereas those behind the RNAP (where DNA is under compression) form closer to it (Fig. 1). We demonstrated that this "action at a distance" can destabilize nucleosomes, leading to DNA unwrapping long before there is any physical contact between the RNAP and the proteins (Fig. 2), which should be relevant in vivo (27, 32).

Our second key finding is that there are two dramatically different modes of supercoiling relaxation in a dsDNA molecule. We observed that twist rapidly diffuses along DNA, and its diffusion constant is about $D_{\mathrm{Tw}} \approx 500\ \mathrm{bp}^2/\tau_{\mathrm{Br}}$. Conversely, writhe, in the form of plectonemes, relaxes much more slowly, and its effective diffusion coefficient is about $D_{\mathrm{Wr}} \approx 1\ \mathrm{bp}^2/\tau_{\mathrm{Br}}$ (consistent with writhe relaxation requiring large-scale DNA rearrangements). Furthermore, writhe relaxation entails at least two characteristic timescales which are associated with the dissipation of internal stress localized at plectonemes, followed by slower relaxation of delocalized writhe. The presence of two relaxation times echoes the behavior of colloidal glasses (33), and it would be intriguing to analyze this parallel further.

Our results may be tested with in vitro experiments with multiple polymerases on plasmids of different size, or with tethered linear DNA in "curtain" arrangements. Topological barriers can be introduced by including DNA-binding proteins which restrict DNA twist, or nonelongating RNAPs. It would also be useful to analyze the relaxation of plectonemic supercoiling and the anomalous diffusion of writhe via imaging techniques such those used in ref. 34, while, by performing experiments on reconstituted chromatin fibers, one could examine whether and when nucleosomes are destabilized or evicted downstream of the advancing RNAP (27). In the future, we suggest it would be desirable to extend this modeling to include the activity of topological enzymes such as topoisomerases (2) and to account for the asymmetry between the major and minor groove which gives rise to a direct coupling between twisting and bending (35, 36), not included in our model.

Materials and Methods

We simulate dsDNA loops using the model described in ref. 15. Each nucleotide is represented by a rigid body formed by a bead and a patch. Beads are connected into a chain, and two chains wind round each other to form a double helix. We use the Large-scale Atomic/Molecular Massively Parallel Simulator (LAMMPS) (37) to perform BD simulations where the position of each nucleotide is determined by a Langevin equation (including terms for internucleotide interactions and an implicit solvent). Full details of the models and how we calculate the various quantities (twist, writhe, local and unsigned writhe, etc.) are given in *SI Appendix*.

Data Availability. All study data are included in the article and/or *SI Appendix*.

ACKNOWLEDGMENTS. This work was supported by the European Research Council (Grant CoG 648050, THREEDCELLPHYSICS). Y.A.G.F. acknowledges support from the Mexican National Council of Science and Technology PhD Grant 384582. D.M. is supported by the Leverhulme Trust (Grant ECF-2019-088).

1. C. R. Calladine, H. Drew, F. B. Luisi, A. A. Travers, E. Bash, *Understanding DNA: The Molecule and How it Works* (Elsevier Academic, 1997), vol. 1.
2. A. Bates, A. Maxwell, *DNA Topology* (Oxford University Press, 2005).
3. J. H. White, Self-linking and the Gauss integral in higher dimensions. *Am. J. Math.* **91**, 693–728 (1969).
4. F. B. Fuller, Decomposition of the linking number of a closed ribbon: A problem from molecular biology. *Proc. Natl. Acad. Sci. U.S.A.* **75**, 3557–3561 (1978).
5. M. Dennis, H. Hannay J, Geometry of Călugăreanu's theorem. *Proc. Math. Phys. Eng. Sci.* **461**, 3245–3254 (2005).
6. Y. Ding *et al.*, DNA supercoiling: A regulatory signal for the λ repressor. *Proc. Natl. Acad. Sci. U.S.A.* **111**, 15402–15407 (2014).
7. C. Naughton *et al.*, Transcription forms and remodels supercoiling domains unfolding large-scale chromatin structures. *Nat. Struct. Mol. Biol.* **20**, 387–395 (2013).
8. M. D. Wang *et al.*, Force and velocity measured for single molecules of RNA. *Science* **282**, 902–907 (1998).
9. E. A. Abbondanzieri, W. J. Greenleaf, J. W. Shaevitz, R. Landick, S. M. Block, Direct observation of base-pair stepping by RNA polymerase. *Nature* **438**, 460–465 (2005).
10. Q. Wang, B. M. Pettitt, Modeling DNA thermodynamics under torsional stress. *Biophys. J.* **106**, 1182–1193 (2014).
11. L. F. Liu, J. C. Wang, Supercoiling of the DNA template during transcription. *Proc. Natl. Acad. Sci. U.S.A.* **84**, 7024–7027 (1987).
12. Y. P. Tsao, H. Y. Wu, L. F. Liu, Transcription-driven supercoiling of DNA: Direct biochemical evidence from in vitro studies. *Cell* **56**, 111–118 (1989).
13. C. A. Brackley *et al.*, Stochastic model of supercoiling-dependent transcription. *Phys. Rev. Lett.* **117**, 018101 (2016).
14. S. A. Sevier, H. Levine, Mechanical properties of transcription. *Phys. Rev. Lett.* **118**, 268101 (2017).
15. Y. A. G. Fosado *et al.*, A single nucleotide resolution model for large-scale simulations of double stranded DNA. *Soft Matter* **12**, 9458–9470 (2016).
16. Y. A. G. Fosado, D. Michieletto, D. Marenduzzo, Dynamical scaling and phase coexistence in topologically constrained dna melting. *Phys. Rev. Lett.* **119**, 118002 (2017).
17. A. Bentivoglio, M. Ancona, C. A. Brackley, G. Gonnella, D. Marenduzzo, Nonequilibrium phase transition in a model for supercoiling-dependent DNA transcription. *Soft Matter* **14**, 3632–3639 (2018).
18. S. P. Mielke, W. H. Fink, V. Krishnan, N. Grønbech-Jensen, C. J. Benham, Transcription-driven twin supercoiling of a DNA loop: A Brownian dynamics study. *J. Chem. Phys.* **121**, 8104–8112 (2004).
19. H. Wada, R. R. Netz, Plectoneme creation reduces the rotational friction of a polymer. *Europhys. Lett.* **87**, 38001 (2009).
20. B. Alberts, A. Johnson, J. Lewis, D. Morgan, M. Raff, *Molecular Biology of the Cell* (Taylor & Francis, 2014).
21. P. R. Cook, *Principles of Nuclear Structure and Function* (John Wiley, New York, 2001).
22. J. Marko, Stretching must twist DNA. *Europhys. Lett.* **38**, 183–188 (2007).
23. J. F. Marko, E. D. Siggia, Bending and twisting elasticity of DNA. *Macromolecules* **27**, 981–988 (1994).
24. F. Kouzine *et al.*, Transcription-dependent dynamic supercoiling is a short-range genomic force. *Nat. Struct. Mol. Biol.* **20**, 396–403 (2013).
25. C. A. Brackley *et al.*, Predicting the three-dimensional folding of cis-regulatory regions in mammalian genomes using bioinformatic data and polymer models. *Genome Biol.* **17**, 31–36 (2015).
26. J. H. White, N. R. Cozzarelli, W. R. Bauer, Helical repeat and linking number of surface-wrapped DNA. *Science* **241**, 323–327 (1988).
27. D. J. Clark, G. Felsenfeld, A nucleosome core is transferred out of the path of a transcribing polymerase. *Cell* **71**, 11–22 (1992).
28. J. F. Marko, Torque and dynamics of linking number relaxation in stretched supercoiled DNA. *Phys. Rev.* **76**, 021926 (2007).
29. D. Michieletto, On the tree-like structure of rings in dense solutions. *Soft Matter* **12**, 9485–9500 (2016).
30. K. Klenin, J. Langowski, Computation of writhe in modeling of supercoiled DNA. *Biopolymers* **54**, 307–317 (2000).
31. P. Nelson, Transport of torsional stress in DNA. *Proc. Natl. Acad. Sci. U.S.A.* **96**, 14342–14347 (1999).
32. N. Gilbert, J. Allan, Supercoiling in DNA and chromatin. *Curr. Opin. Genet. Dev.* **25**, 15–21 (2014).
33. M. Medina-Noyola, Long-time self-diffusion in concentrated colloidal dispersions. *Phys. Rev. Lett.* **60**, 2705 (1988).
34. M. T. van Loenhout, M. de Grunt, C. Dekker, Dynamics of DNA supercoils. *Science* **338**, 94–97 (2012).
35. S. K. Nomidis, F. Kriegel, W. Vanderlinden, J. Lipfert, E. Carlon, Twist-bend coupling and the torsional response of double-stranded DNA. *Phys. Rev. Lett.* **118**, 217801 (2017).
36. E. Skoruppa, S. K. Nomidis, J. F. Marko, E. Carlon, Bend-induced twist waves and the structure of nucleosomal DNA. *Phys. Rev. Lett.* **121**, 088101 (2018).
37. S. Plimpton, Fast parallel algorithms for short-range molecular dynamics. *J. Comput. Phys.* **117**, 1–19 (1995).